Optical and Quantum Electronics (2023) 55:456
https://doi.org/10.1007/s11082-023-04718-8

Structural, optical, photoluminescence and magnetic investigation of doped and Co-doped ZnO nanoparticles

A. Sedky[1] · N. Afify[1] · Abdullah Almohammedi[2] · E. M. M. Ibrahim[3] · Atif Mossad Ali[4]

Received: 26 April 2022 / Accepted: 24 February 2023 / Published online: 2 April 2023

Abstract

We report here the structural, optical, photoluminescence (PL), and magnetic investigation of $Zn_{1-x-y}Fe_xM_yO$ nanoparticles. The lattice constants and crystallite size are decreased by Fe, followed by a further decrease up to (Fe + M) = 0.30. A compressive stress is approved and the size of particle is between 180 and 277 nm and follows the sample order of ZnO, (Fe + Cu), (Fe + Ni), and Fe. Although a single value of energy gap (E_g) is found for pure and Fe-doped ZnO, two values of E_g (E_{gh} and E_{gl}) are found for the co-doped samples. The E_g is generally increased by Fe, followed by a further increase for the Cu-series, whereas it is decreased for the Ni-series. The refractive indices n_K and n_T proposed by different methods are generally decreased by Fe, followed by a further decrease for both series. Although Fe doped ZnO depressed the density of carriers (N/m*), it increased again for the co-doped samples. The residual dielectric constant ϵ_L is decreased by Fe, followed by an increase for the Cu-series, but it is decreased for the Ni-series. The loss factor tan δ increases slightly with Fe, followed by an increase for the Ni-series, but it decreases in the Cu-series. A significant depression of optical conductivity σ_{opt} by Fe was obtained, followed by a further decrease which is higher for the Cu-series. The PL shows four visible emissions. Interestingly, an IR emission at about 825 nm is only obtained for the co-doped samples. Furthermore, the blue emission (I_{blue}) was higher than UV (I_{UV}), [$(I_{blue}/I_{UV}) > 1$], but it is greater for the Ni series than the Cu. Although ZnO exhibits diamagnetic behavior, the Fe and co-doped samples exhibit ferromagnetic with higher magnetization for the Ni-series than the Cu. The current results recommend the co-doped samples in nanoscale for some of advanced devices.

Keywords XRD analysis · Optical constants · PL emission · RTFM · Optoelectronics · Spintronic

✉ A. Sedky
sedky196000@hotmail.com; sedky1@aun.edu.eg

Extended author information available on the last page of the article

1 Introduction

The n-type ZnO has been used in optoelectronic, gas sensor, solar cell, and spintronic devices due to its stability at ambient conditions. (Manikandan et al. 2017; Ragupathi et al. 2013; Padmapriya et al. 2016; Ali and Hakeem 2015). Additionally, ZnO can be used as a specific component in magneto, photo, spin-electronics, and microwave devices when Zn is doped by 3-d transition metals (TM) (Mustaqima and Liu 2014; Djerdj et al. 2010; Yang 2013). Unfortunately, further research is still needed for the co-doped ZnO as compared with individual dopants.

The electron–hole (e–h) pairs are generated when the valence band (VB) electrons are excited by absorbing of photons (Othman et al. 2017). ZnO holds towards blue and UV optical devices due to their wide band gap E_g (3.2 eV) of ZnO and larger Urbach energy (60–100 meV) (Liu et al. 2010; Tariq et al. 2019). The UV-blue photoluminescence (PL) band emission of ZnO represents the near band edge (NBE) of charge carriers. The NBE emission can be delineated as a photo-excitation of charge carriers from VB to CB, resulting in an exciton (e–h pairs) formation and subsequent radiative recombination of e–h pairs. In addition, ZnO with additives exhibits good PL centres due to their multi-color emission, which is necessary for white light emitting diodes (LEDs) (Poornaprakasha et al. 2020; Xu and Cao 2009). This is why the PL spectrum of ZnO is characterized by two main peaks (a sharp UV peak at 380 nm and broad deep band emission between (400–600 nm) (Shan et al. 2004; Sedky et al. 2022). The broad deep band emission is due to deep centers, which are caused by intrinsic and extrinsic defects. In addition, some of whole visible region of different coloured could be obtained by defects (Wang et al. 2006).

In order to create ferromagnetic (FM) at a high Curie temperature (T_C) close to RT for spintronic devices, ZnO doped with TM have been early used (Mohamed et al. 2023a). RTFM is caused by exchange spin interaction between free delocalized carriers and localized TM (Kittilstved et al. 2005).Therefore, a lot of work has been investigated through the magnetic moment of ZnO: TM as well as the stable polarized state exhibited by TM (Mohamed et al. 2023b; Sedky et al. 2022a). The T_c in ZnO: TM is very sensitive to phase purity, doping type and morphologies. However, the T_c has decreased when ZnO co-doped with magnetic ions like Co, Mn, Fe, and Ni (Mandal et al. 2006; Zhang et al. 2007). Likewise the RTFM are affected by oxygen vacancies (Ahmed 2017). For clarifying the origin of RTFM, the ZnO co-doped by two different ions in nanoscale will be presented.

The recent advancement of various quantum size effects in nanotechnology implies that the majority of novel devices are based on pure and co-doped ZnO nanomaterial by shrinking their size to the nanoscale (Aljaafari and Sedky 2020; Dutta et al. 2003; Lopez-Quintela et al. 2003). For example, the optical absorption properties of ZnO nanoparticles are found to be more suitable for many optical devices due to their significant UV reflection as compared to ZnO micro-particles. These are beneficial for ZnO applications in skin care products, optical devices, dye-sensitized and solar cells (Jadhav et al. 2013; Amin and Sedky 2019; Zhang et al. 2016; Karmakar et al. 2010; Wojnarowicz et al. 2015). Unfortunately, further research is required for more advantage for the high stability of co-doped ZnO to be satisfied for advanced devices (Wojnarowicz et al. 2016; Neena et al. 2016).

Recently, Sedky et al. presented a comparative study on the structural and optical properties of $Zn_{0.90-x}Fe_xM_yO$ bulk ceramics (Abdullahi et al. 2015; Al-Naim et al. 2021a, 2021b). Unlike the articles mentioned, the particle size has been minimized and structural, optical, PL, and RTFM properties are well evaluated. Regardless of the behavior of the obtained parameters against co-doping content, the phase purity of ZnO was improved,

the crystallite size was decreased to about 10 nm and ZnO bond length was increased from 1.974 Å to 2.064. Å. The micro-strain was increased two times and the residual stress was changed from tensile to compressive like-behavior. Interestingly, the average size of nanoparticle domains or grain agglomerations was depressed to a few hundred nanometers and did not exceed 400 nm.

2 Experimental details

$Zn_{1-x-y}Fe_xM_yO$ samples with various M, x,y were synthesized by using the solid-state reaction method. The powders of ZnO, Fe_2O_3, CuO and NiO are mixed and calcined in air for 16 h at 950 °C. ZnO, Zn0.1Fe, Zn0.1FeCu0.05, Zn0.1FeCu0.10, Zn0.1FeCu0.20, Zn0.1FeNi0.05, Zn0.1FeNi0.10, and Zn0.1FeNi0.20 were sintered at 1000 °C for 16 h before being slowly cooled to RT. The (Fe + Cu) samples are called the Cu series for simplicity, whereas the (Fe + Ni) are called the Ni series. After that, the sizes of the pellets with equal quantities are minimized to the nanometer scale by a mechanical ball milling machine (200 rpm rotation speed and 20-min duration time). The phase purity and particle size are respectively tested by XRD using Cu-Kα radiation and JEM (1230 TEM) with a 100 kV. The optical properties were tested against wavelength (200–1000 nm) using double beam UV–visible-NIR spectrophotometer (Jasco V-570, Japan). The PL measurements are made by Jasco FP-6500 spectrofluorometer of 150-W Xenon arc lamp and 5 nm bandwidths. The emission spectra were measured at an excitation wavelength of 300 nm. Finally, magnetic measurements (M(H) loops) of the samples were taken using vibrating sample magnetometer (VSM Lakeshore 7410) over a field range of up to + 10 KOe.

3 Results and discussion

3.1 Structural analysis

The XRD patterns of the samples shown in Fig. 1 indicated that most of peaks belong to ZnO wurtzite structure [ICSD 01–079-0208 (space group P63mc)]. The ZnO and Zn0.1FeNi0.05 samples are free from any extra lines, while an extra line with little intensity is formed for the remaining samples as listed in Table 1. The 2θ-angles of the extra lines are about 53.26°, 39.82°, and 42.88° for Fe, Cu series, and Ni series, respectively. The average intensities I_{avg} of the (100), (002), and (111) intense lines listed in Table 1 are decreased by Fe, followed by an increase as co-doping increases to 0.10 and then decreases to 0.20, but they are higher for the Cu series than the Ni. Lattice constants a and c, and unit cell volume V listed in Table 1 are reduced by Fe, followed by a further reduce as the content of co-doping increases, but they are higher for the Cu series than the Ni (Sedky 2014; Chow et al. 2013; Aksoy et al. 2010; Seetawan et al. 2011; Wojnarowicz et al. 2018; Sedky and Mohamed 2014). The size of crystallite D_{hkl} given by; $D_{hkl} = \frac{K\lambda}{\beta \cos\theta}$ (Sedky 2014) and listed in Table 1, is decreased by Fe doping, followed by a further decrease as the content of co-doping increases to 0.10 and then increases to 0.20, but it is higher for the Ni series than the Cu. The micro strain ε_m calculated by; $\varepsilon_m = \frac{\beta \cos\theta}{4}$, and listed in Table 1 is increased by Fe, followed by an increase with more co-doping content to 0.10, and then a decrease to 0.20, but it is higher for the Cu series than the Ni as reported (Sedky 2020; Muhammad et al. 2019; Srinivasulu et al. 2017). However, the lattice strain ε_L given by; ε_L

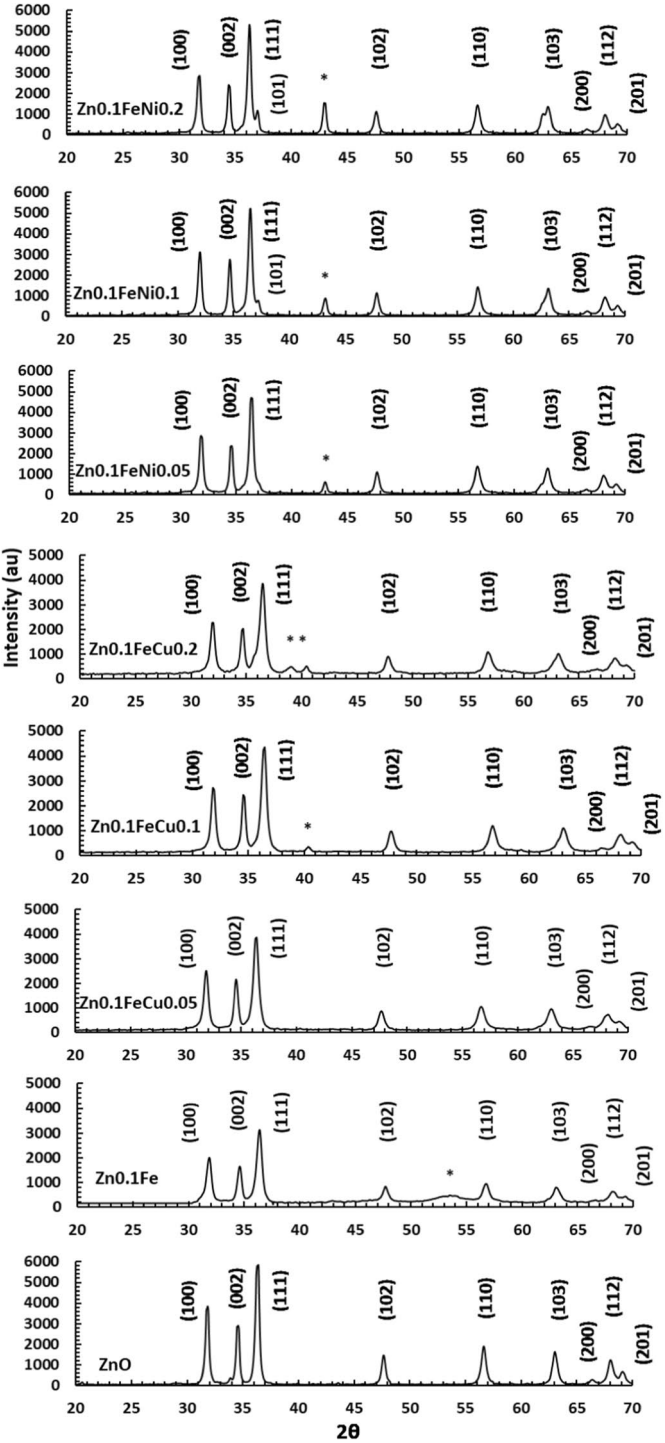

Fig. 1 XRD patterns for the samples

Table 1 2Θ-angles, average intensity (I_{avg}), lattice parameters (a, c), unit cell volume (V), crystallite size (D_{hkl}), grain size (D_{TEM}), microstrain (ε_m), lattice strain (ε_L) and residual stress (σ) for the samples

Sample	2Θ	I_{avg} (au)	a (Å)	c (Å)	V $(Å)^3$
ZnO	–	4106.3	3.387	5.447	54.108
Zn0.1Fe	53.26	2059.7	3.384	5.441	53.969
Zn0.1FeCu0.05	–	2768	3.381	5.438	53.838
Zn0.1FeCu0.10	39.82	3140.7	3.376	5.432	53.608
Zn0.1FeCu0.20	38.44 39.94	2629.7	3.378	5.445	53.842
Zn0.1FeNi0.05	42.88	3181	3.378	5.435	53.718
Zn0.1FeNi0.10	42.88	3693.1	3.373	5.429	53.479
Zn0.1FeNi0.20	42.88	3489.3	3.375	5.443	53.681
Sample	D_{hkl} (nm)	D_{TEM} (nm)	$\varepsilon_L \times 10^{-2}$	$\varepsilon_m \times 10^{-3}$	σ (Gpa)
ZnO	14.72	180	4.63	2.36	− 10.781
Zn0.1Fe	14.14	295	4.52	2.46	− 10.523
Zn0.1FeCu0.05	13.09		4.47	2.65	− 10.395
Zn0.1FeCu0.10	12.54	266	4.34	2.77	− 10.095
Zn0.1FeCu0.20	15.15	–	4.61	2.29	− 10.781
Zn0.1FeNi0.05	13.98	–	4.39	2.48	− 10.223
Zn0.1FeNi0.10	13.07	277	4.28	2.66	− 9.966
Zn0.1FeNi0.20	15.83	–	4.56	2.20	− 10.609

$= \frac{c-c_o}{c_o}$ and listed in Table 1, has the inverse behavior ($c_o = 5.2066$ Å for unstrained ZnO) (Srinivasan and Kannan 2015). The residual stress σ is determined by Rusu et al. (2011); Mukhtar et al. 2012);

$$\sigma = \frac{[2S_{13}^2 - S_{33}(S_{11} + S_{12})]\varepsilon}{2S_{13}} = -232.8\varepsilon_L \quad (1)$$

S_{13}, S_{33}, S_{11} and S_{12} equal to 104.2, 213.8, 208.8 and 119.7 GPa for ZnO. The σ values listed in Table 1 for the two series indicate compressive stress.

The micrographs and histograms of the ZnO, Zn0.1Fe, and Zn0.1FeCu0.1and Zn0.1FeNi0.1 samples shown in Fig. 2 contain agglomerations of different shapes and sizes of irregular grains. The sizes of grains are between (150–400 nm), (250–1500 nm), (200–800 nm) and (200–1000 nm). The sizes (D_{TEM}) against the high counts of particles are 180, 295, 266, and 277 nm, inconsistent with those obtained for D_{hkl}. This means that D_{hkl} and D_{TEM} are respectively controlled by the ionic size and the ability of the nanoparticles agglomerations, which generally follow the order of (Fe + Cu), (Fe + Ni) and Fe.

3.2 Optical measurements

Figure 3a–c plots absorbance (A) against wavelengths (λ). It is seen that A was decreased by Fe-doping, and then decreases for the Cu series, while it increased for the Ni series. It is expected that some of the shallow levels are introduced inside the band gap by (Fe + Cu) co-doping, and consequently, the absorption edge exhibits a red

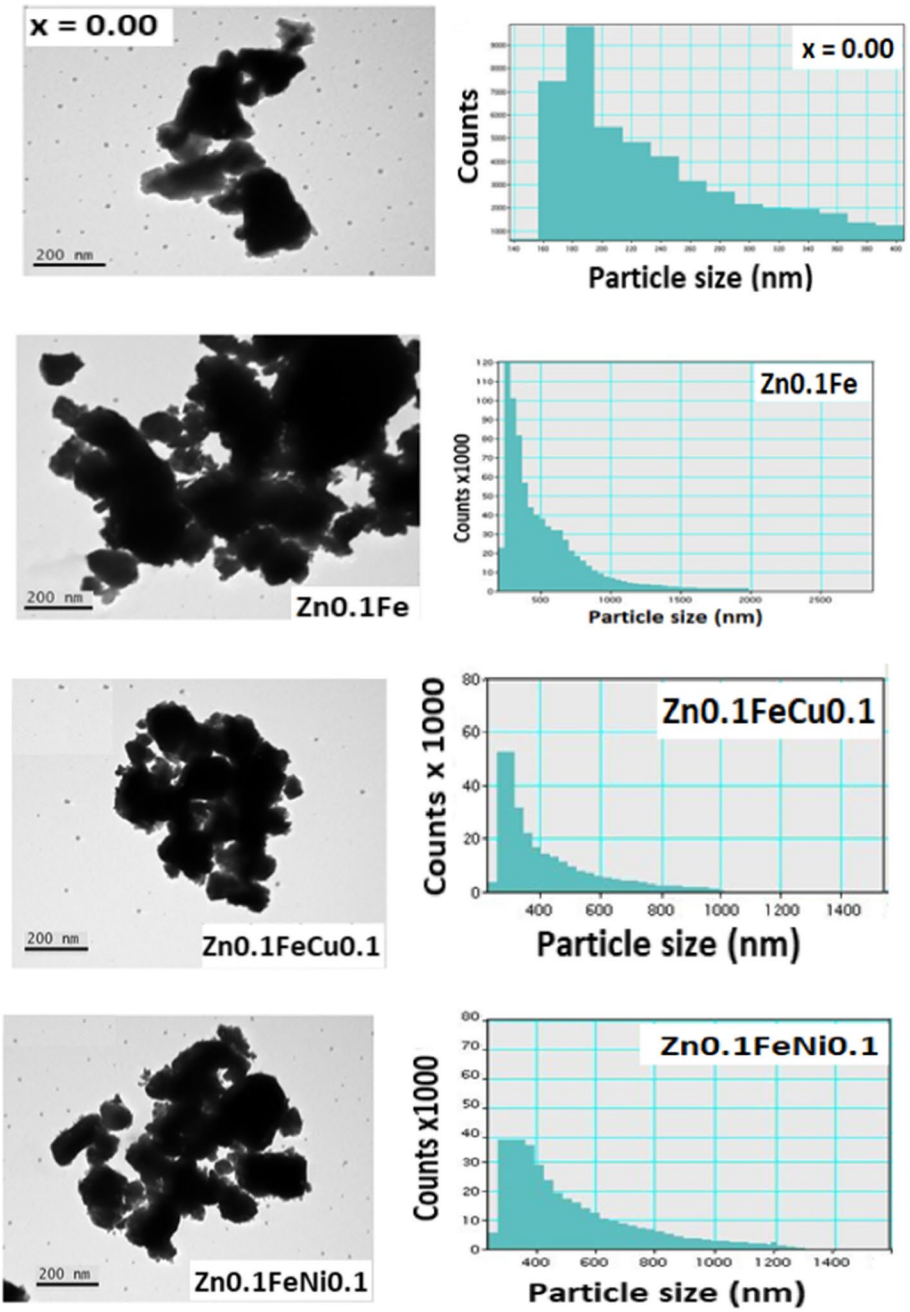

Fig. 2 TEM graphs for the Zn0.1Fe, Zn0.1FeCu$_{0.1}$ and Zn0.1FeNi0.1 nanoparticles agglomerations

shift as Cu content increases. However, the vice is versa for the Ni series. Two optimum regions of A close to or below 400 nm are evident for all samples, owing to a significant increase in A as λ decreases. The second maximum, however, is missing

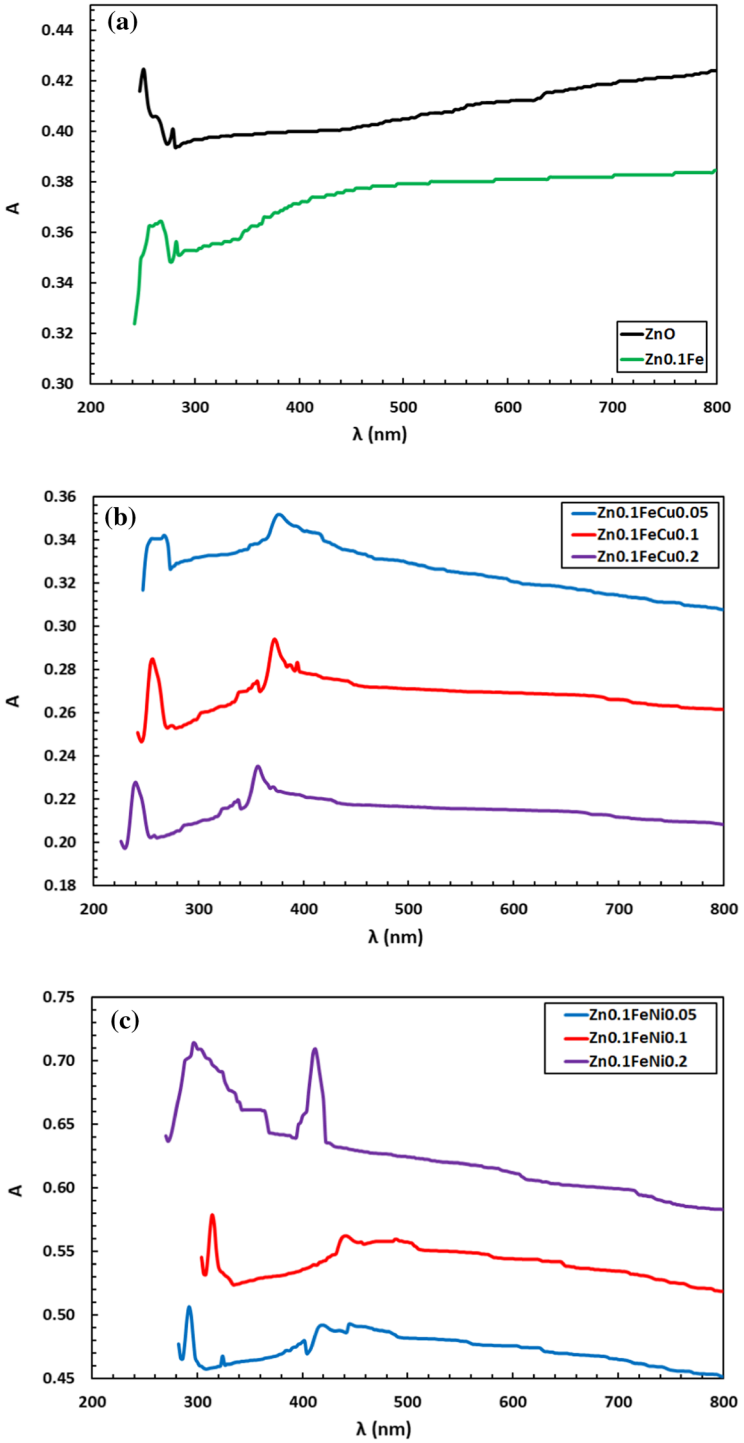

Fig. 3 **a** Absorbance (A) as a function of wavelength (λ) for the samples. **b** Absorbance (A) as a function of wavelength (λ) for the samples. **c** Absorbance (A) as a function of wavelength (λ) for the samples

from the A- curves for pure and Fe samples. This is due to increasing free carrier density as the λ decreases towards near-UV ~ 400 nm (exciton peaks) (Ali et al. 2005). As given in Table 2, the A_{max} occurs at λ $(1)_{max}$ = 249, 256 nm for pure and Fe samples and decreases to 253, 251, 238 nm for the Cu-series, but it is increased to 292, 314, 294 nm for the Ni series. The second A_{max} is obtained at λ $(2)_{max}$ = 379, 368, 354 nm for the Cu-series and 414, 436, 410 nm for the Ni series. This means that the required energy for creating the e–h pairs is generally increased by Cu, but it is also increased by Ni.

The absorption coefficient α is determined by, α = 2.303 ln(A/t), where t is the cuvette diameter. Therefore, the E_g was obtained for allowed direct transition using Taucs equation (Abdalla et al. 2003; Wang et al. 2003);

$$(\alpha h\upsilon)^{\frac{1}{m}} = A(h\upsilon - E_g) \tag{2}$$

However, the plot of $(\alpha h\upsilon)^2$ against the hυ is used to get the E_g (see Fig. 4a–c). Two significant absorption edges are only observed for the co-doped samples of both series, indicating two electronic transitions. The values of E_g of the first and second transitions are called E_{gh} and E_{gL} since that ($E_{gh} > E_{gL}$).

The values of E_{gh} and E_{gl} listed in Table 2 and shown in Fig. 5 are generally increased by Fe, followed by a further increase for the Cu-series up to (Fe + M) = 0.30. While, they increased for the Ni-series at (Fe + M) = 0.15 Ni followed by a decrease up to (Fe + M) = 0.30. The $\Delta E = (E_{gh} - E_{gl})$ values are respectively 1.60, 1.40, 1.52 eV for the Cu-series and 0.85, 0.90, 0.25, eV for the Ni series, in which ΔE decreases as M increases, but it is higher for the Cu series than the Ni. Anyhow, two E_g are also recorded for n-type semiconductors (Sedky et al. 2019; Ismail et al. 2011). However, the decrease in E_g for the Ni-series may be due to some defects formed in the host materials, thereby creating insulating states in the forbidden gap inside the band structure. While the increase in E_g for the Cu-series may be due to producing high carrier concentration, some of them may be blocked, and increases the E_g as obtained, which is required for high power operation (Yu et al. 2001; Sagadevan et al. 2017a).

Additionally, the refractive indices (n_T and n_K) are examined in terms of E_g as follows (Kumar and Singh 2010; Tripathy 2015);

Table 2 Wavelengths (λ_1, λ_2) against maximum absorbance, energy gaps (E_{gh}, E_{gL}), refractive indices (n_K, n_T), carrier density (N/m*) and residual dielectric constant (ϵ_L) for the samples

Sample	λ(1) $_{max}$ (nm)	λ(2) $_{max}$ (nm)	E_{gh} (eV)	E_{gL} (eV)	n_K	n_T	(N/m*) × 10^{55} (g cm^{-3})	ϵ_L
ZnO	249	–	3.02	–	2.567	2.376	3.69	9.445
Zn0.1Fe	256	–	3.42	–	2.471	2.251	0.62	5.587
Zn0.1FeCu0.05	253	379	3.80	2.20	2.188	2.154	3.69	6.328
Zn0.1FeCu0.10	251	368	3.90	2.50	2.169	2.132	1.23	9.178
Zn0.1FeCu0.20	238	354	4.22	2.70	2.111	2.063	1.23	12.55
Zn0.1FeNi0.05	292	414	3.70	2.85	2.209	2.178	1.23	3.147
Zn0.1FeNi0.10	314	436	3.55	2.65	2.239	2.216	1.23	2.318
Zn0.1FeNi0.20	296	410	3.75	2.50	2.199	2.165	1.23	1.626

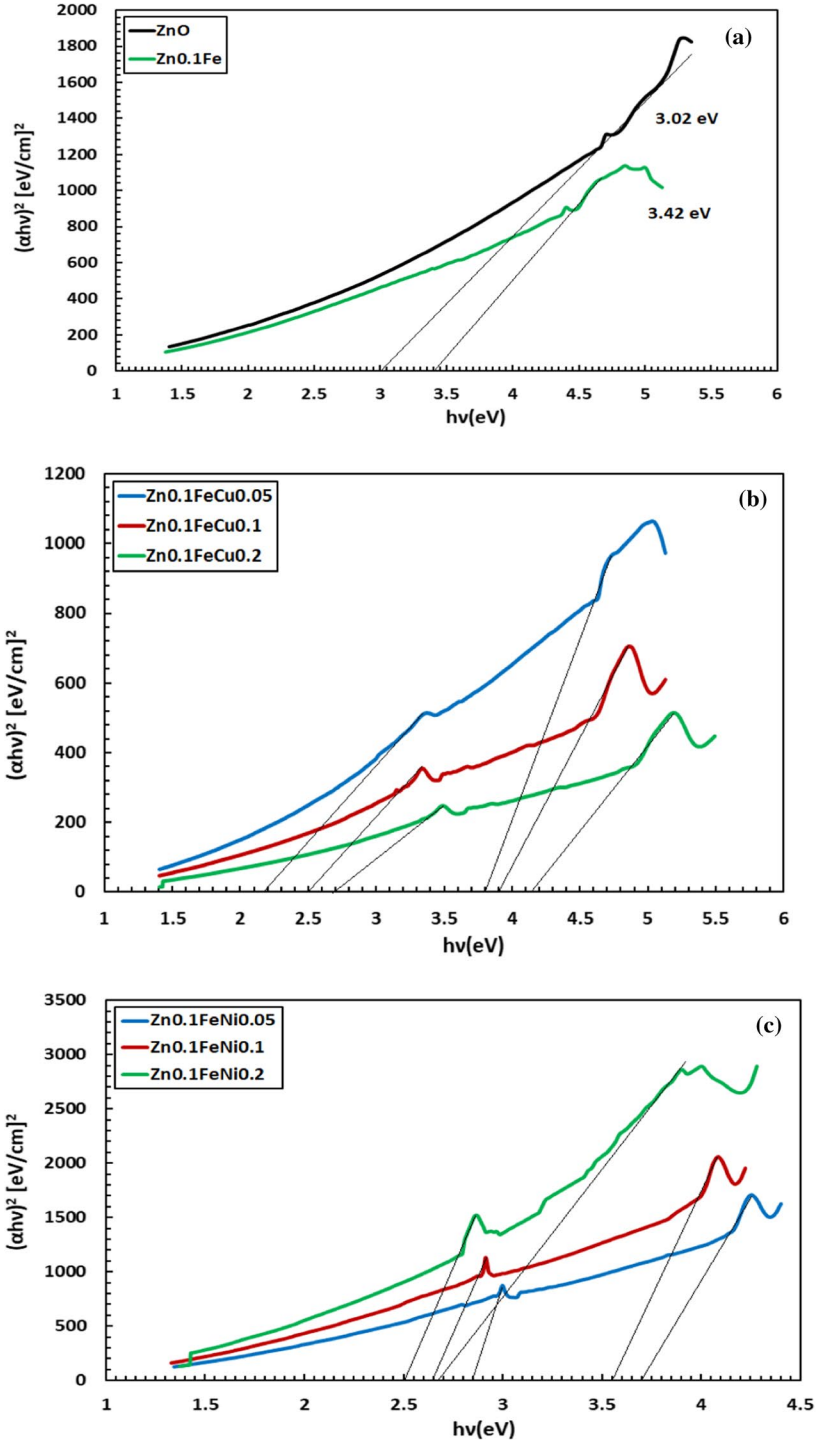

Fig. 4 **a** $(\alpha h\nu)^2$ as a function of photon energy ($h\nu$) for ZnO and $Zn_{0.1}Fe$ samples. **b** $(\alpha h\nu)^2$ as a function of photon energy ($h\nu$) for the (Fe + Cu) samples. **c** $(\alpha h\nu)^2$ as a function of photon energy ($h\nu$) for the (Fe + Ni) samples

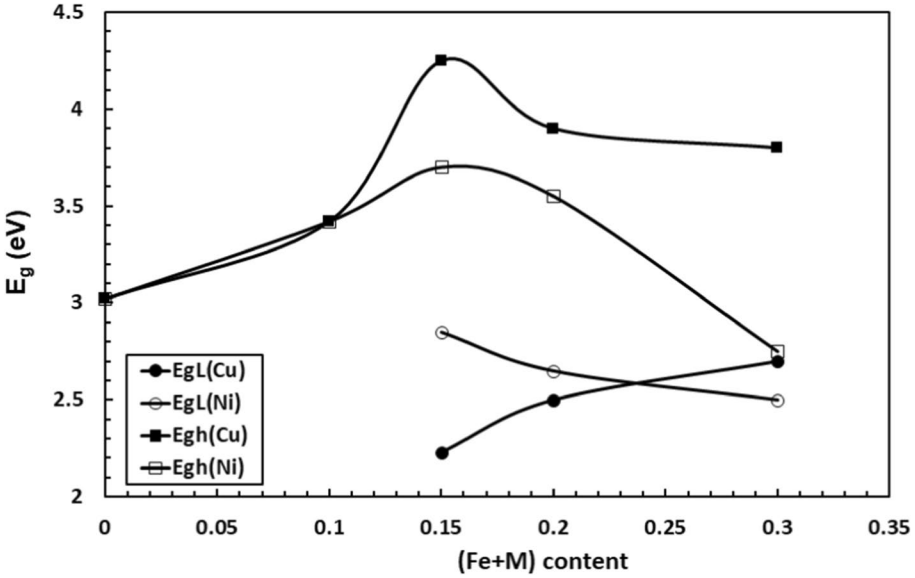

Fig. 5 Energy gap as a function of (Fe + M) content for the samples

$$\begin{aligned} n_K &= 3.367E_g^{-0.323} \\ n_T &= 1.73[1 + 1.902\exp(-0.539E_g)] \end{aligned} \tag{3}$$

where n_K and n_T are the refractive indices proposed by V. Kumar and S. K. Tripathy empirical methods. Since the E_{gL} values are not obtained for pure and Fe samples, we have simply used the values of E_{gh}. The n_K, and n_T values listed in Table 2 are decrease by Fe, followed by a further decrease for both co-doped series, but the values of n_K are higher than those of n_T.

The lattice dielectric constant represents the n against λ is determined by Abdel-Khalek et al. (1178); Zeyada et al. 1960):

$$\begin{aligned} (n^2 - k^2) &= \in_L - \left(\frac{e^2}{4\pi^2 c^2 \varepsilon_0}\right)\left(\frac{N}{m^*}\right)\lambda^2 \\ k &= \frac{\alpha\lambda}{4\pi}; n = \frac{1+R}{1-R} \pm [\frac{4R}{(1-R)^2} - k^2]^{\frac{1}{2}} \end{aligned} \tag{4}$$

where c, e, ε_o, m*, N, k and R denote light speed, free space permittivity, charge and effective mass of an electron, free carrier density, extinction coefficient and reflectance, respectively. The (n^2-k^2) against λ^2 plot shown in Fig. 6a give the ϵ_L and N/m* as listed in Table 2 and also shown against (Fe + M) content in Fig. 6b, c. The Fe doped ZnO depressed the (N/m*) from 3.69×10^{55} to 0.62×10^{55} ($g.cm^{-3}$), but it increased again to 1.23×10^{55} ($g.cm^{-3}$) for the co-doping, which slightly supports them for the use of optoelectronic. However, a significant increase of (N/m*) for the 0.85Zn0.1Fe0.05Cu sample is not clear at present, but it may related to the clean phase purity of the samples as indicated in the XRD analysis. This behavior indicates that the electronic polarization of ZnO is generally reduced by co-doping for both series, as reported (El-Desoky et al. 2014). ϵ_L was decreased by Fe, followed by an increase for the Cu-series, but it is decreased for the Ni-series as well

as E_g. The increase/decrease of ϵ_L as M increases for the Cu/Ni- series, can be attributed to oxygen vacancies (Lin et al. 2013).

The optical (σ_{opt}) and electrical (σ_{elec}) conductivities can be evaluated by Sedky et al. (2021);

$$\sigma_{opt} = \frac{\alpha nc}{4\pi}$$
$$\sigma_{ele} = \frac{2\lambda\sigma_{opt}}{\alpha} \quad (5)$$

The behavior of both σ_{opt} and σ_{elec} with the photon energy $h\nu$ for the samples is shown in Fig. 7a, b. σ_{opt} is almost the same with increasing $h\nu$ to 3 eV, but it slightly increases above this energy. In contrast, a significant depression of 0.1 Fe was obtained, followed by a further decrease for both series, but the rate of decrease was higher for the Cu-series than the Ni. The value is reduced from 5.5×10^{10} s^{-1} for ZnO to 4×10^{10} s^{-1} for a 0.9Zn0.1Fe sample. On the other hand, σ_{ele} has regular behavior, but its values are 10^4 times lower than σ_{opt}. In addition, it was decreased by 0.1Fe, followed by an increase for the Cu-series, but it decreased for the Ni. This trend is due increasing the free carriers by co-doping which support the conductivity.

Furthermore, the dependence of dissipation factor tan δ on the real ε_r ($\varepsilon_r = n^2 - k^2$) and imaginary part ε_i ($\varepsilon_i = 2nk$) of dielectric constant, according to the following relation (Mott 1970; Mohamed et al. 2019; Moustafa et al. 2019);

$$\tan\delta == \frac{\varepsilon_i}{\varepsilon_r} \quad (6)$$

As shown in Fig. 8, the tan δ slightly increases by Fe, followed by a further increase for the Ni-series up to M = 0.30, whereas it decreases for the Cu-series. In addition, it is generally decreased when increasing the $h\nu$ for all samples. However, increasing the quality factor (q = (1/ tan δ) for the Cu-series is required for the use of super-capacitor, while its decrease for the Ni-series is convenient for normal capacitors.

3.3 Photoluminescence (PL) measurements

The PL intensity of the samples shown in Fig. 9a, b shows four visible emissions which are required for light emitting diodes. Interestingly, an extra five IR emission peak is obtained only for the co-doped samples. As listed in Table 3, a little bit of shift to higher/lower values of λ as the content of co-doping M increases could be observed, but not exceed 9 nm (λ_{UV}, λ_{blue}, λ_{green}, λ_{red}, λ_{IR} are the wavelengths against the PL emission peaks, respectively). Further, the doping has decreased the PL of ZnO, but it is higher for the Ni series than the Cu, which can be considered evidence of more states of defects induced by the co-doping, due to reducing the crystalline quality of the ZnO with M content. However, there are two very sharp near-UV and blue peaks recorded at 409 and 464.5 nm for ZnO and 410.5 and 466 nm for Zn0.1Fe samples. In addition, they are recorded between (411.5–415 nm), (467.5–469 nm) for the Cu series and between (401–407 nm), (459.5–467 nm) for the Ni series. However, the PL of blue (I_{blue}) is always higher than that of UV (I_{UV}), as shown in Fig. 9c, [(I_{blue}/I_{UV}) > 1], but it is higher for the Ni series than the Cu.

However, the UV emissions (3.088–2.991 eV) are related to the E_g of ZnO, whereas the visible are due intrinsic defects of the vacancies and interstitials of both O and Zn (V_o, V_{Zn}, O_i Zn_i) (Vanheusden et al. 1996; Fan et al. 2005). The violet emissions are controlled

Fig. 6 **a** Refractive index (n^2-k^2) as a function of wavelength (λ) for the samples. **b** Lattice dielectric constant (ϵ_L) as a function of (Fe + M) content for the samples. **c** Carrier density (N/m*) as a function of (Fe + M) content for the samples

by the transition of electron from Zn_i shallow donor (~0.40 eV under CB) to the highest of VB (Tatsumi et al. 2004). The blue emission (2.702–2.647 eV) is due to radiative transition of an electron from Zn_i shallow donor to V_{Zn} acceptor (Heo et al. 2005). The highest broad peak of green emission (2.288–2.241 eV) is caused by recombination of donor V_{o-} by acceptor V_{Zn} (Murphy et al. 2006; Sedky and Mohamed 2013).The red emission (2.027–1.988 eV) is attributed to the co-doped ZnO (Sagadevan et al. 2017b; Sedky et al. 2012). The lowest IR emission, (1.516–1.499 eV) is due to excitation of (3d/4f) lowest state, in consistent with ZnO doped by Tm^{3+} (Jadwisienczak et al. 2002). However, the obtained emissions are good evidence that the co-doped ions are successfully incorporated into ZnO as reported (El-Said Bakeer 2020; Layek et al. 2016; Van Dijken et al. 2000; Van Dijken et al. 2000; Xu et al. 2009; Mohamed et al. 2021).

3.4 RTFM measurements

Figure 10a, b depicts the magnetization of the samples against a magnetic field (M-H). ZnO exhibits perfect diamagnetic behavior as reported, whereas clear ferromagnetic is obtained for both series (Ateia et al. 2015). The hysteresis loop for Fe samples (0.9Zn0.1Fe) is weak and, therefore, it can be classified ferromagnetic or super-magnetic. Interestingly, the magnetization was increased with the further addition of M up to 0.20 (co-doped samples), but it is higher for the Ni-series than the Cu. But with an increase of M to 0.30, a decrease in magnetization has occurred for both series. The magnetization of the Ni series decreased, but is still higher than that of M = 0.20 (0.8Zn0.1FeNi0.05). In contrast, it is depressed for the Cu-series and becomes similar to the Fe sample (0.9Zn0.1Fe). The saturated magnetization M_s versus M content shown in Fig. 11a and listed in Table 4 was not obtained for ZnO due to diamagnetic behavior. However, it becomes 0.171, 0.238, 0.296, 0.178 (emu/g) for the Cu-series, and 0.171, 0.291, 0.450, 0.343 (emu/g) for the Ni-series. Although M_s was decreased for M = 0.30 samples of both series, it was still higher than that of Fe samples, especially for the Ni-series.

To be more specific, the M_s = [M_s (co-doped)-(M_s (Fe)] values listed in Table 4 are 0.067, 0.125, and 0.007 (emu/g) for the Cu-series and 0.12, 0.279, and 0.172 (emu/g) for the Ni-series.

Firstly, the decrease of M_s for M = 0.30 sample in both series is related to the XRD extra lines as a result of solubility limit discussed above. This behavior indicates that RTFM is controlled by the degree of phase purity obtained through synthesis and co-doping content. Secondly, Ni is ferromagnetic with effective magnetic moment ($\mu = 2.83\mu_B$). When Zn^{+2} are replaced by Ni^{+2} in either tetrahedral or octahedral coordination, the T_c of ZnO are controlled by the interaction of Ni bound magnetic poltroons within the localized spins and free carriers (oxygen vacancies). Nevertheless, it has reported by the authors that M_s of 0.20 Ni doped ZnO is about 0.085 (emu/g) (El-Bassuony and Abdelsalam 2017), which is 5-times lower than of (0.8Zn0.1FeNi0.10), and indicating strong mutual participation between localized spin of co-doping of Fe and Ni as compared to individual doping by Fe or Ni even in case of decreasing (N/m*) for Ni-series stated above. Although Cu is perfect diamagnetic, M_s of Cu-series are 1.7-times more than of Fe, which is very interesting point. This is due increasing N/m* of

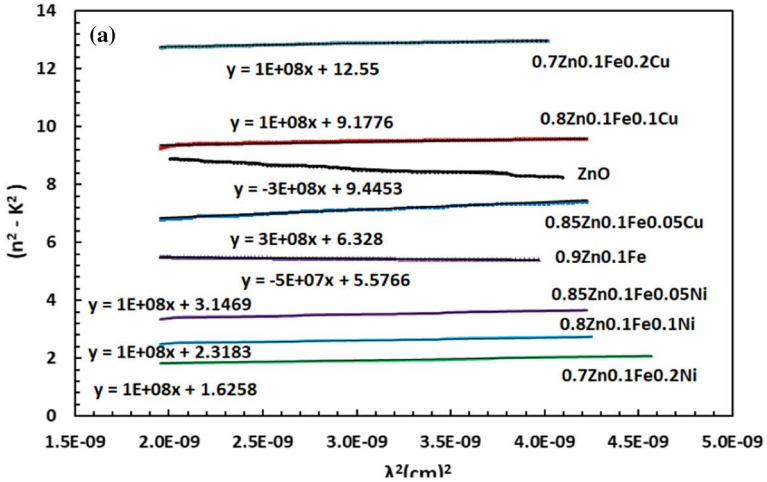
(a)
y = 1E+08x + 12.55
0.7Zn0.1Fe0.2Cu
y = 1E+08x + 9.1776
0.8Zn0.1Fe0.1Cu
ZnO
y = -3E+08x + 9.4453
0.85Zn0.1Fe0.05Cu
y = 3E+08x + 6.328
0.9Zn0.1Fe
y = -5E+07x + 5.5766
0.85Zn0.1Fe0.05Ni
y = 1E+08x + 3.1469
0.8Zn0.1Fe0.1Ni
y = 1E+08x + 2.3183
0.7Zn0.1Fe0.2Ni
y = 1E+08x + 1.6258
(n² - K²)
λ²(cm)²

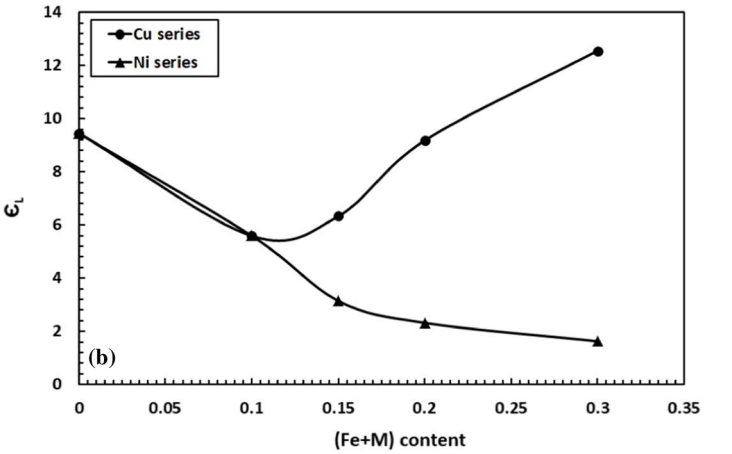
Cu series
Ni series
(b)
(Fe+M) content

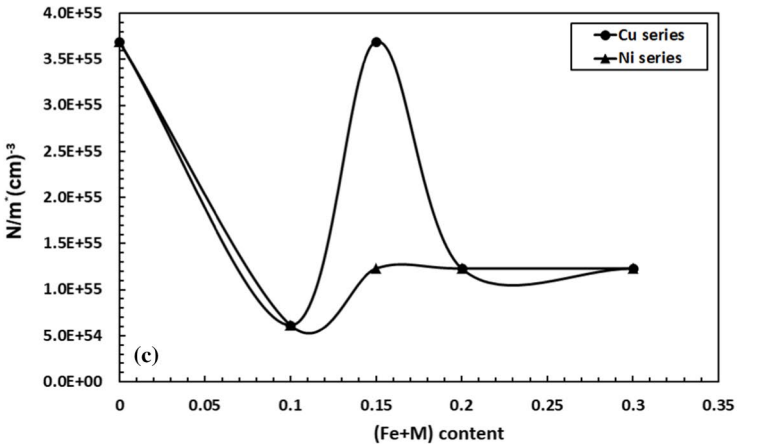
Cu series
Ni series
(c)
N/m*(cm)⁻³
(Fe+M) content

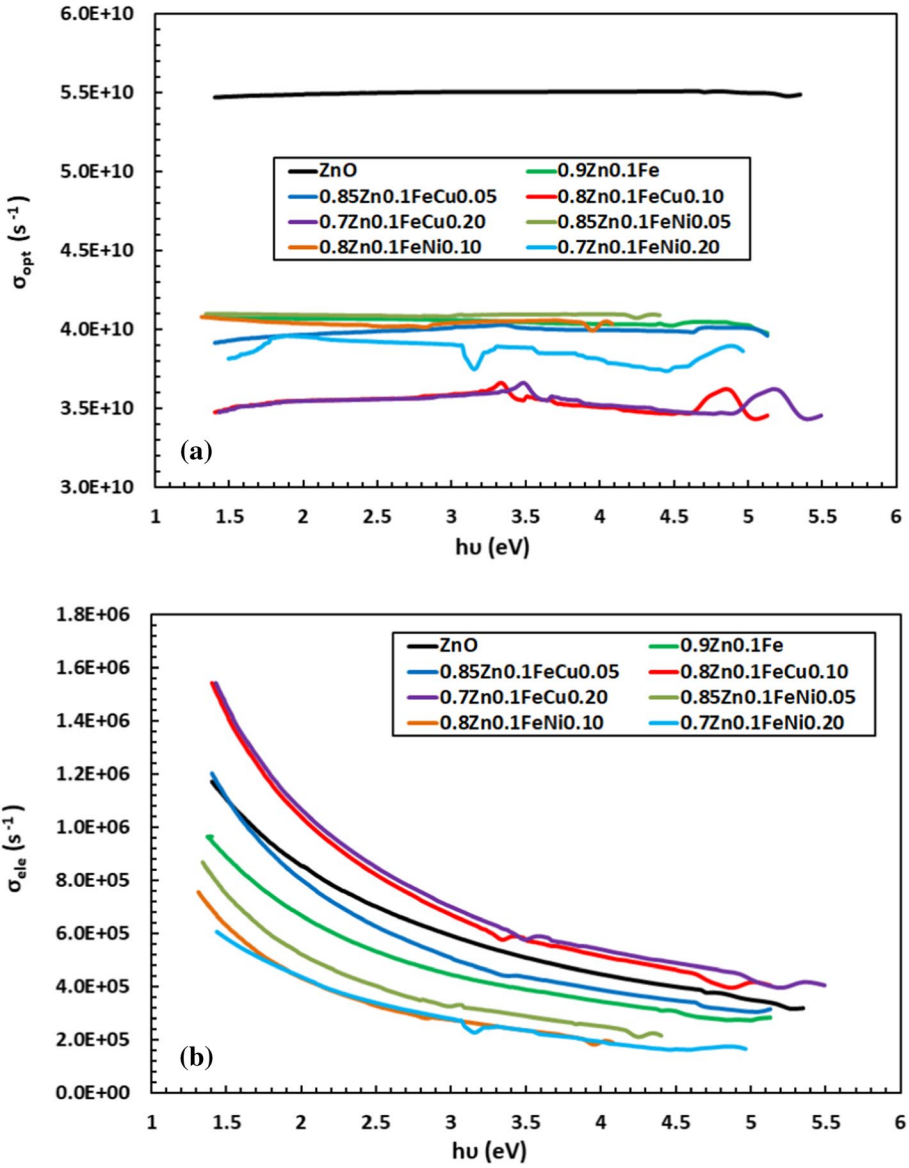

Fig. 7 **a** Optical conductivity (σ_{opt}) as a function of photon energy ($h\nu$) for the samples. **b** Electrical conductivity (σ_{opt}) as a function of photon energy ($h\nu$) for the samples

Cu-series, which may also increase the mutual interaction between Fe localized spin and free carriers. To support our thinking, the M_s of Cu-series is about 1.5 lower than of Ni-series, which indicates that RTFM of ZnO is controlled by the introduced free carriers beside the localized spin of TM. To our knowledge, M_s of 0.7Zn0.1FeCu0.20 was decreased to 0.178 (emu/g), which is approximately similar to Fe doping, 0.171 (emu/g).

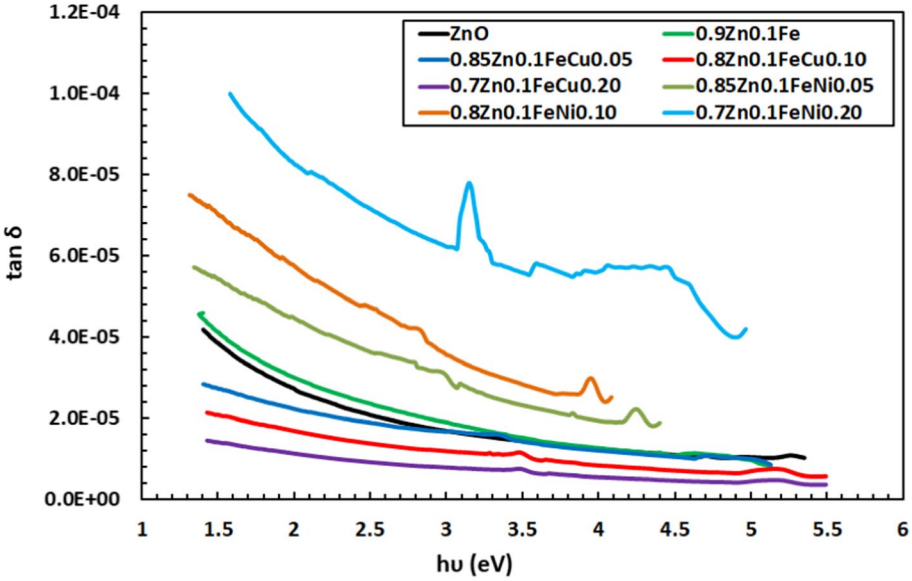

Fig. 8 Dissipation factor (tan δ) as a function of photon energy ($h\nu$) for the samples

However, the coercivity of the field (H_c), remnant magnetization (M_r), magnetization width (ΔM), squareness ($S_q = M_r/M_s$), M-H straight line slope (dc susceptibility χ_{dc}), magnetic moment calculated by; ($WM_s/5585$) and magnetic anisotropy factor γ given by; ($H_cM_s/0.98$) (Srinet et al. 2013; Coey et al. 2008) are listed in Table 4. Furthermore, the M-H straight line slope (dc susceptibility χ_{dc}) versus M is also shown in Fig. 11b. All of them are increased by the co-doping, but they are higher for the Ni-series than the Cu, which strongly supports the RTFM for all doped and co-doped samples as expected. (Coey and Chambers 2008; Samanta et al. 2018). The observed ferromagnetism at RT seems to be the combined effect of the interaction of TM spin at the tetrahedral sites with charge carriers of oxygen vacancies to form bound magnetic polarons (Coey and Chambers 2008; Samanta et al. 2018; Mohamed et al. 2022; Yong-Sheng et al. 2010).

Recently, the RTFM of ZnO can also be enhanced through a co-doping mechanism (Ram and Negi 2016; Sedky et al. 2022b). For example, an induced RTFM could be obtained as Fe increases in $Zn_{1-x}Co_{0.05}Fe_xO$, but unfortunately it is lower than that of $Zn_{1-x}(Fe+Cu)_xO$ [95–96]. They indicate that $Zn_{1-xx}Cu_{0.05}Fe_xO$ does not have a tendency to form the Fe–O-Co ferromagnetic cluster. In contrast, $Zn_{1-x}(Fe+Cu)_xO$ has a tendency to form the Fe–O-Cu ferromagnetic cluster of the double-exchange mechanism with the charge transfer between Fe and Cu. Although this behavior inconsistent with the present work, all of them are correct because they fixed the Co/Cu content at 0.05 and increased the Fe content. Regardless, the local spin of Fe, which increases for both series, the rate of interaction, of Fe induced spin with charge carrier due to Cu-ion, is higher than Fe + Co induced spin with charge carrier. This will eventually support the conflict with our work, which strongly highlights the present investigation.

Let us now compare the present analysis with those reported but in microscale (Chow et al. 2013). Firstly, the phase purity of ZnO was improved and the V was increased from (46.397–47.876 $Å^3$) to (53.479–54.108 $Å^3$). While the average crystallite size, D_{hkl}, was decreased from about 26 nm to about 10 nm. The ε_m was increased to twice times and

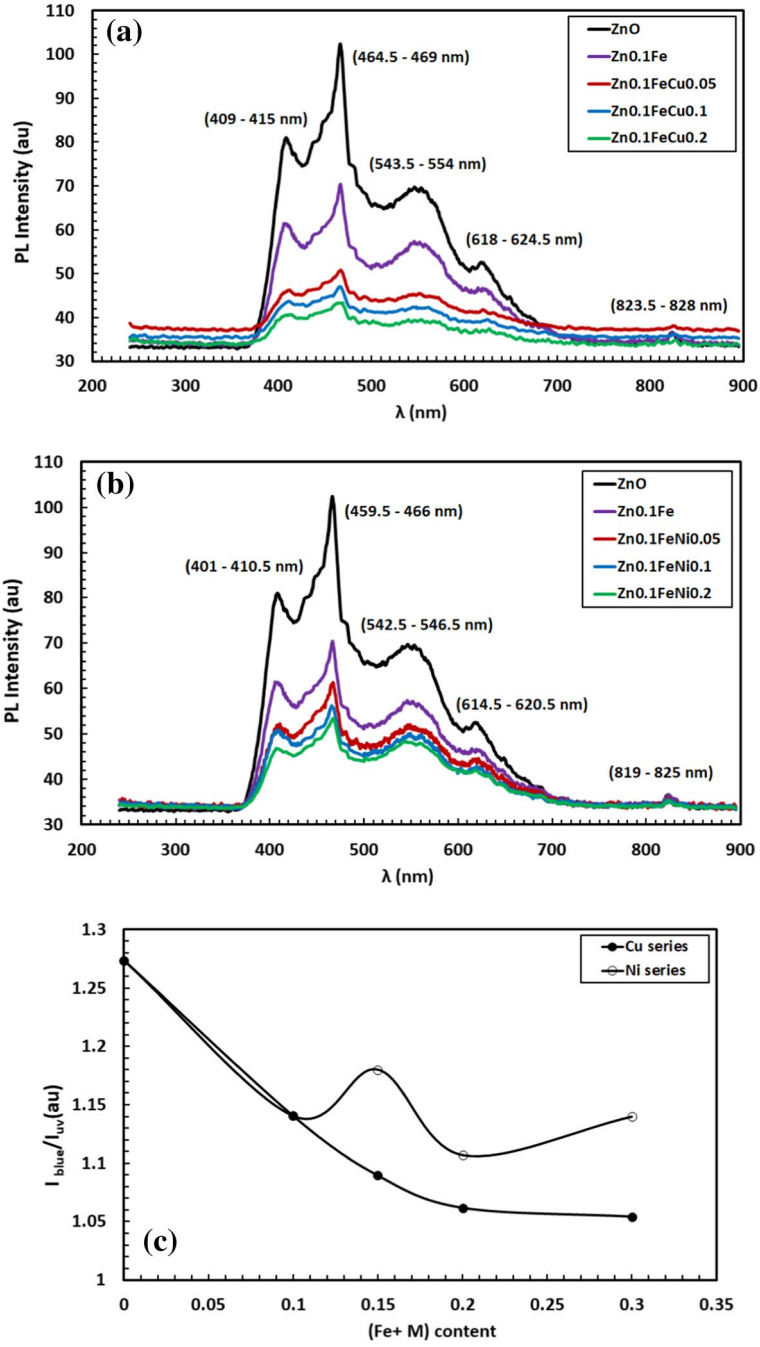

Fig. 9 **a** PL intensity as a function of wavelength for the pure and (Fe + Cu) samples **b** PL intensity as a function of wavelength for the pure and (Fe + Ni) samples. **c** The blue shift (I_{blue}/I_{uv}) as a function of (Fe + M) content for the samples

Table 3 The wavelengths of UV, blue, green, red and IR against PL emission peaks, and the I_{UV} and I_{blue} for the samples

Sample	λ_{UV} (nm)	λ_{blue} (nm)	λ_{green} (nm)	λ_{red} (nm)	λ_{IR} (nm)	I_{uv} (au)	I_{blue} (au)
ZnO	409	464.5	543.5	618	–	79.892	101.752
Zn0.1Fe	410.5	466	546.5	620.5	–	60.447	68.938
Zn0.1FeCu0.05	411.5	467	548.5	621.5	826	45.191	49.238
Zn0.1FeCu0.10	413	468.5	551.5	623	827.5	42.988	45.65
Zn0.1FeCu0.20	415	469	554	624.5	828	40.365	42.559
Zn0.1FeNi0.05	407	467	546.5	618.5	823	51.139	60.353
Zn0.1FeNi0.10	403.5	463.5	544	612.5	820.5	49.118	55.007
Zn0.1FeNi0.20	401	459.5	542.5	614.5	819	44.973	54.308

the residual stress was transferred from tensile to compressive like-behavior. Interestingly, the D_{TEM} was depressed to a few hundred nanometers not exceed 300 nm, which is about 8-times lower than D_{SEM}. Interestingly, the λ_{max} and the E_g were shifted to lower values. They are decreased form (264–340 nm), (2.851–3.974 eV) to (249–314 nm), (3.02–3.88 eV). Moreover, two E_g are obtained for the co-doped samples. Similar behavior was obtained for the (N/m*) and ϵ_L which they were also decreased from (0.86×10^{55}–221.40×10^{55} ($g.cm^{-3}$)), (1.96–23.96) to (0.62×10^{55}–3.96×10^{55} ($g.cm^{-3}$)) and (1.626–12.55). Based on the above, we concluded that the behaviors of materials nanoscale are convenient for most of advanced applications rather than microscale.

4 Conclusion

Structural, optical, photoluminescence, and magnetic properties of $Zn_{1-x-y}Fe_xM_yO$ nanoparticles were investigated. The average nanoparticle size is between 180 and 277 nm and follows the sample order of ZnO, (Fe + Cu), (Fe + Ni) and Fe. Two values of E_g are for the co-doped samples. The E_g was increased by the co-doping, but it is higher for the Cu-series than for Ni. Similar behavior is obtained for (N/m*), ε_L and q-factor. A blue shift [$(I_{blue}/I_{UV}) > 1$] is obtained for all samples, but it is higher for the Ni series than the Cu. A noticeable RTFM is clearly obtained for the Fe and co-doped samples with evaluated magnetization parameters. These findings strongly recommend the (Fe + Cu) series in nanoscale for high power operation, solar cell and supercapacitor devices. In contrast, the (Fe + Ni) series is recommended for light-emitting diodes and spintronics.

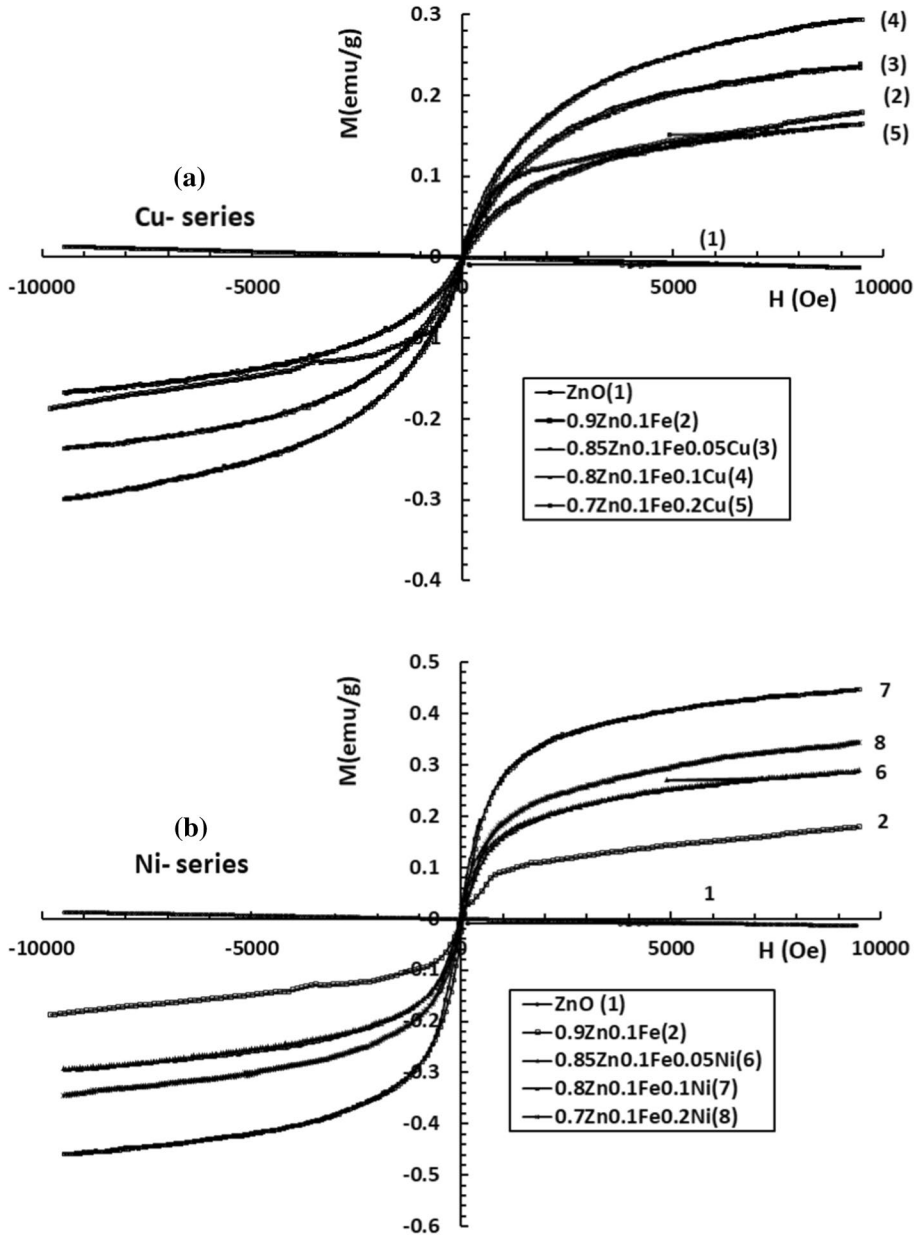

Fig. 10 **a** Magnetization (M) as a function of magnetic field (H) for pure and (Fe + Cu) series. **b** Magnetization (M) as a function of magnetic field (H) for pure and (Fe + Ni) series

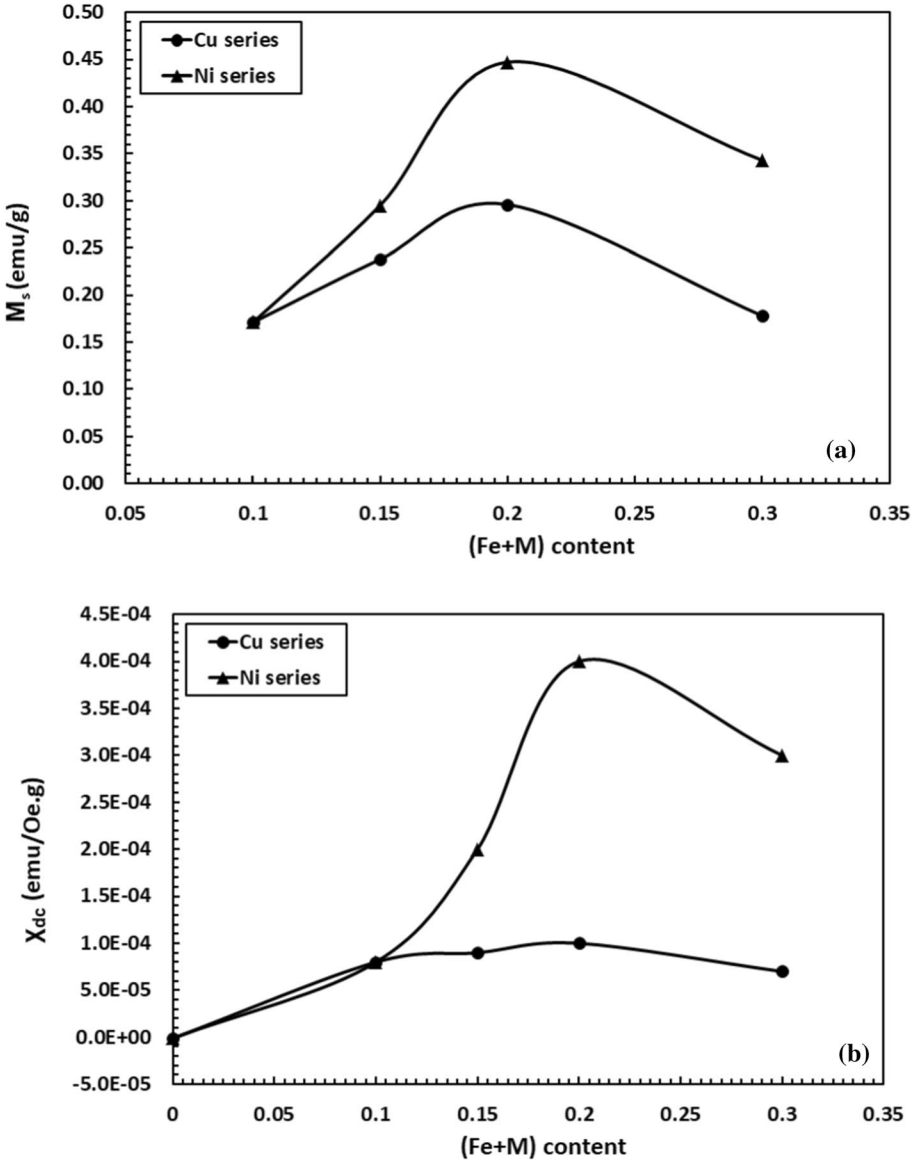

Fig. 11 **a** Saturated magnetization (M_s) as a function of (Fe + M) content for the samples. **b** dc magnetic susceptibility (χ_{dc}) as a function of (Fe + M) content for the samples

Table 4 Coercivity (H_c), dc magnetic susceptibility (χ_{dc}), saturated magnetization (M_s), magnetization width (ΔM), remnant magnetization (M_r), squareness (Sq), magnetic anisotropy (γ) and magnetic moment (μ) for $Zn_{1-x-y}Fe_xM_yO$ samples

Sample	H_c (Oe)	χ_{dc} (emu/g. Oe)	M_s (emu/g)	ΔM_s (emu/g)	M_r (emu/g)	Sq	γ (Oe. emu)/g	μ (μ_B)
ZnO	–	−1E−6	–	–	–	–	–	–
Zn0.1Fe	17.25	8E−5	0.171	–	0.0017	0.01	3.01	0.002
Zn0.1FeCu0.05	40.87	9E−5	0.238	0.067	0.0055	0.023	9.926	0.003
Zn0.1FeCu0.10	41.80	1E−4	0.296	0.125	0.0077	0.026	12.63	0.004
Zn0.1FeCu0.20	34.50	7E−5	0.178	0.007	0.0038	0.021	6.266	0.003
Zn0.1FeNi0.05	37.10	2E−4	0.295	0.120	0.0133	0.045	11.17	0.004
Zn0.1FeNi0.10	47.50	4E−4	0.447	0.279	0.023	0.051	21.67	0.006
Zn0.1FeNi0.20	51.85	3E−4	0.343	0.172	0.022	0.064	18.15	0.005

Funding Open access funding provided by The Science, Technology & Innovation Funding Authority (STDF) in cooperation with The Egyptian Knowledge Bank (EKB). The authors have not disclosed any funding.

Data availability The datasets generated and analyzed during the current study will be available from the corresponding author on reasonable request, but after acceptance.

Declarations

Conflict of interest The authors declare that the present work is original not published or submitted elsewhere, and they have never conflict of interest.

References

Abdalla, S., Easawi, K., El-Brolossy, T.A., Yossef, G.M., Negm, S., Talaat, H.: Determination of thermophysical parameters of porous silicon using a photothermal technique. Rev. Sci. Instrum. **74**(1), 848 (2003)

Abdel-Khalek, H., Shalaan, E., Abd-El Salam, M., El-Sagheer, A.M., El-Mahalawy, A.M.: Effect of thermal annealing on structural, linear and nonlinear optical properties of 1, 4, 5, 8-naphthalene tetracarboxylic dianhydride thin films. J. Mol. Struct. **1178**, 408–419 (2019)

Abdullahi, S.S., Köseog, Y., Güner, S., Kazan, S., Kocaman, B., Ndikilar, C.E.: Synthesis and characterization of Mn and Co codopedZnO nanoparticles. Superlattices Microstruct. **83**, 342–352 (2015)

Ahmed, S.A.: Structural, optical, and magnetic properties of Mn-doped ZnO samples. Results Phys. **7**, 604–610 (2017)

Aksoy, S., Caglar, Y., Ilican, S., Caglar, M.: Temperature dependence of the optical band gap and electrical conductivity. Chem. Eng. Civ. Eng. Mech. Eng. **227** (2010)

Ali, H.M., Hakeem, A.M.: Characterization of n and p-type (SnO2)x (ZnO)1–x nanoparticles thin films. Eur. Phys. J. Appl. Phys. **72**(1), 10301 (2015)
Ali, H.M., Mohamed, H.A., Mohamed, S.H.: Enhancement of the optical and electrical properties of ITO thin films deposited by electron beam evaporation technique. Eur. Phys. J. Appl. Phys. **31**, 87 (2005)
Aljaafari, A., Sedky, A.: Influence of fine crystal percentage on the electrical properties of ZnO ceramic-based varistors. Curr. Comput.-Aided Drug Des. **10**(8), 681 (2020)
Al-Naim, A.F., Sedky, A., Afify, N., Ibrahim, S.S.: Structural, FTIR spectra and optical properties of pure and co-doped Zn1-x-y FexMyO ceramics with (M= Cu, Ni) for plastic deformation and optoelectronic applications. Appl. Phys. a. **127**, 1–20 (2021a)
Al-Naim, A.F., Afify, N., Sedky, A., Ibrahim, S.S.: Structural morphology and nonlinear behavior of pure and co-doped $Zn_{1-x-y}Fe_xM_yO$ varistors with (M= Cu, Ni). Appl. Phys. A **127**(7), 486 (2021b)
Amin, A., Sedky, A.: On the correlation between electrical, optical and magnetic properties of $Zn_{1-x}Pr_xO$ nanoparticles. Mater. Res. Express **6**, 065903 (2019)
Ateia, E.E., Salah, L.M., El-Bassuony, A.A.H.: Synthesis and characterization of EPDM/ferrite. Inorg. Organomet. Polym. Mater. **25**, 1362 (2015)
Chow, L., Lupan, O., Chai, G., Khallaf, H., Ono, L.K., Cuenya, B.R., Tiginyanu, I.M., Ursaki, V.V., Sontea, V., Schulte, A.: Synthesis and characterization of Cu-doped ZnO one-dimensional structures for miniaturized sensor applications with faster response. Sens. Actuators A Phys. **189**, 399–408 (2013)
Coey, J.M.D., Chambers, S.A.: Oxide dilute magnetic semiconductors—fact or fiction. MRS Bull. **33**, 1053 (2008)
Coey, J.M.D., Wongsaprom, K., Alaria, J., Venkatesan, M.: Charge-transfer ferromagnetism in oxide nanoparticles. J. Phys. D Appl. Phy. **41**, 134012 (2008)
Djerdj, I., Jaglici, Z., Arcon, D., Niederberger, M.: Co-doped ZnO nanoparticles: minorreview. Nanoscale **2**, 1096–1104 (2010)
Dutta, A., Gayathri, N., Ranganathan, R.: Effect of particle size on the magnetic and transport properties of La0.875Sr0.125MnO3. Phys. Rev. B **68**, 054432 (2003)
El-Bassuony, A.A.H., Abdelsalam, H.K.: Giant exchange bias of hysteresis loops on Cr3+-doped Ag Nanoparticles. J. Supercond. Nov. Magn. (2017). https://doi.org/10.1007/s10948-017-4340-x
El-Desoky, M.M., Ali, M.A., Afifi, G., Imam, H.: Annealing effects on the structural and optical properties of growth ZnO thin films fabricated by pulsed laser deposition (PLD). J. Mater. Sci. Mater. Electron. **25**, 5071–5077 (2014). https://doi.org/10.1007/s10854-014-2273-8
El-Said Bakeer, D.: Elastic study and optical dispersion characterization of Fe-substituted cobalt aluminate nanoparticles. Appl. Phys. A **126**, 443 (2020)
Fan, X.M., Lian, J.S., Zhao, L., Liu, Y.: Single violet luminescence emitted from ZnO films obtained by oxidation of Zn film on quartz glass. Appl. Surf. Sci. **252**, 420–424 (2005)
Heo, Y.W., Norton, D.P., Pearton, S.J.: Origin of green luminescence in ZnO thin film grown by molecular-beam epitaxy. J. Appl. Phys. **98**, 073502 (2005)
Ismail, R.A., Ali, A.K., Ismail, M.M., Hassoon, K.I.: Preparation and characterization of colloidal ZnO nanoparticles using nanosecond laser ablation in water. Appl. Nanosci. **1**, 45–49 (2011)
Jadhav, J., Patange, M., Biswas, S.: Ferromagnetic Ni-doped ZnO nanoparticles synthesized by a chemical precursor method. Carbon Sci. Tech. **5**(2), 269 (2013)
Jadwisienczak, W.M., Lozykowski, H.J., Xu, A., Patel, B.: Visible emission from ZnO doped with rare-earth ions. J. Electron. Mater. **31**, 776–784 (2002)
Karmakar, D., Rao, T.C., Yakhmi, J.V., Yaresko, A., Antonov, V.N., Kadam, R.M., Mandal, S.K., Adhikari, R., Das, A.K., Nath, T.K., Ganguli, N.: Electronic structure and magnetic properties of (Fe, Co)-codoped ZnO: theory and experiment. Phys. Rev. B **81**(18), 184421 (2010)
Kittilstved, K.R., Norberg, N.S., Gamelin, D.R.: Chemical manipulation of high-TC ferromagnetism in ZnO diluted magnetic semiconductors. Phys. Rev. Lett. **94**, 147209 (2005)
Kumar, V., Singh, J.K.: Model for calculating the refractive index of different materials. Indian J. Pure Appl. Phys. **48**, 571 (2010)
Layek, A., Banerjee, S., Manna, B., Chowdhury, A.: Synthesis of rare-earth doped ZnO nanorods and their defect–dopant correlated enhanced visible-orange luminescence. RSC Adv. **6**(42), 35892–35900 (2016)
Lin, C.P., Chen, H., Nakaruk, A., Koshy, P., Sorrell, C.C.: Efect of annealing temperature on the photocatalytic activity of TiO2 thin flms. Energy Procedia **34**, 627–636 (2013)
Liu, X.C., Chen, Z.Z., Zhen, B.Z.C., Shi, E.W., Liao, D.Q.: Structural, optical and electrical properties of Ga-doped and (Ga, Co)-co-doped ZnO films. J. Cryst. Growth **312**, 2871–2875 (2010)
Lopez-Quintela, M.A., Hueso, L.E., Rivas, J., Rivadulla, F.: Intergranular magnetoresistance in nanomanganites. Nanotechnology **14**, 212–219 (2003)

Mandal, S.K., Das, A.K., Nath, T.K., Karmakar, D.: Temperature dependence of solubility limits of transition metals (Co, Mn, Fe, and Ni) in ZnO nanoparticles. Appl. Phys. Lett. **89**, 144105 (2006)

Manikandan, A., Manikandan, E., Meenatchi, B., Vadivel, S., Jaganathan, S.K., Ladchumananandasivam, R., Henini, M., Maaza, M., Aanand, J.S.: Rare earth element (REE) lanthanum doped zinc oxide (La:ZnO) nanomaterials: synthesis structural optical and antibacterial studies. J. Alloys Compd **723**, 1155–1161 (2017)

Mohamed, M., Abdelraheem, A.M., Abd-Elrahman, M.I., Hadia, N.M.A., Shaaban, E.R.: Composition dependence of structural and linear and non-linear optical properties of CdS1−xMnx semiconducting thin films. Appl. Phys. A **125**(7), 483 (2019)

Mohamed, M., Sedky, A., Alshammari, A.S., Gandouzi, M.: Optical, photoluminescence and ferromagnetic properties of Ni-doped ZnO for optoelectronic applications. J. Mater. Sci. Mater. Electron. **32**, 5186–5198 (2021)

Mohamed, M., Sedky, A., Alshammari, A.S., Alshammari, M.S., Khan, Z.R., Bouzidi, M., Gandouzi, M.: Structural, FTIR, optical, mechanical and magnetic properties of Zn1−xFexO with various Fe nanopowder additions. Appl. Phys. A **128**(5), 408 (2022)

Mohamed, M., Sedky, A., Alshammari, A.S., Khan, Z.R., Bouzidi, M.: Structural and nonlinear I-V characteristics of co-substituted Sn1− x− yZnxMyOz varistors with various x, y and M. J. Electron. Mater. **52**, 2514–2524 (2023a)

Mohamed, M., Sedky, A., Alshammari, A.S., Khan, Z.R., Bouzidi, M., Gandouzi, M.: Structural, morphological, optical, photocatalytic activity investigations of Bi doped ZnO nanoparticles. Opt. Mater. **136**, 11334 (2023b)

Mott, N.F.: Conduction in non-crystalline systems: IV. Anderson localization in a disordered lattice. Philos. Mag. **22**(175), 7–29 (1970)

Moustafa, S., Mohamed, M., Abdel-Rahim, M.A.: Composition dependence of structural and optical properties of Ge_xSe_{100-x} semiconducting thin filmsOpt. Quantum Electron. **51**, 337 (2019)

Muhammad, W., Ullah, N., Haroon, M., Abbasi, B.H.: Optical, morphological and biological analysis of zinc oxide nanoparticles (ZnO NPs) using *Papaver somniferum* L,. RSC Adv. **9**(51), 29541–29548 (2019)

Mukhtar, M., Munisa, L., Saleh, R.: Co-precipitation synthesis and characterization of nanocrystalline zinc oxide particles doped with Cu2+ Ions. Mater. Sci. Appl. **3**, 543 (2012)

Murphy, T.E., Moazzami, K., Phillips, J.D.: Trap-related photoconductivity in ZnO epilayersJ. Electron. Mater. **35**, 543–549 (2006)

Mustaqima, M., Liu, C.: ZnO-based nanostructures for diluted magnetic semiconductor. Turk. J. Phys. **38**, 429–441 (2014)

Neena, D., Shah, A.H., Deshmukh, K., Ahmad, H., Fu, D.J., Kondamareddy, K.K., Kumar, P., Dwivedi, R.K., Sing, V.: Influence of (Co-Mn) co-doping on the microstructures, optical properties of sol-gel derived ZnO nanoparticles. Eur. Phys. J. D **70**, 53 (2016)

Othman, A., Othman, M.A., Ibrahim, E.M.M., Ali, M.A.: Sonochemically synthesized ZnO nanosheets and nanorods: annealing temperature efects on the structure, and optical properties. Ceram. Int. **43**, 527–533 (2017)

Padmapriya, G., Manikandan, A., Krishnasamy, V., Jaganathan, S.K., Antony, S.A.: Enhanced catalytic activity and magnetic properties of spinel MnxZn1-xFe2O4 nano-photocatalysts by microwave irradiation route. J. Supercond. Novel Magn. **29**, 2141 (2016)

Poornaprakasha, B., Chalapathia, U., Subramanyamb, K., Vattikutic, S.V.P., Park, S.H.: Wurtzite phase Co-doped ZnO nanorods: Morphological, structural, optical, magnetic, and enhanced photocatalytic characteristics. Ceram. Int. **46**, 2931–2939 (2020)

Ragupathi, C., Vijaya, J.J., Manikandan, A., Kennedy, L.J., Ragupathi, C., Vijaya, J.J., Manikandan, A., Kennedy, L.: Phytosynthesis of nanoscale ZnAl2O4 by using sesamum (Sesamum indicum L) optical and catalytic properties. J. Nanosci. Nanotechnol. **13**(12), 8298–8306 (2013)

Ram, M., Negi, N.S.: Effect of (Fe, Co) co-doping on the structural, electrical and magnetic properties of ZnO nanocrystals prepared by solution combustion method. Phys. B Condens. Matter. **481**, 185–191 (2016)

Rusu, D., Rusu, G., Luca, D.: Structural characteristics and optical properties of thermally oxidized zinc films. Acta Phys. Polon. A **119**(6), 850–856 (2011)

Sagadevan, S., Pal, K., Chowdhury, Z.Z., Hoque, M.E.: Structural, dielectric and optical investigation of chemically synthesized Ag-doped ZnO nanoparticles composites. J. Sol-Gel Sci. Technol. **83**, 394–404 (2017a)

Sagadevan, S., Pal, K., Chowdhury, Z.Z., Hoque, M.E.: Structural, dielectric and optical investigation of chemically synthesized Ag-doped ZnO nanoparticles composites. J. Sol-Gel Sci. Technol. **83**(2), 394–404 (2017b)

Samanta, A., Goswami, M.N., Mahapatra, P.K.: Magnetic and electric properties of Ni-doped ZnO nanoparticles exhibit diluted magnetic semiconductor in nature. J. Alloys Compd. **730**, 399–407 (2018)
Sedky, A.: Effects of Bi_2O_3 addition in micro and nano scale on the structural and electrical properties of $Zn_{1-x}Bi_xO$ varistors. Braz. J Phys. **44**(4), 305–414 (2014)
Sedky, A., Mohamed, S.B.: Effect of temperature on the electrical properties of $Zn_{0.95}$ $M_{0.05}O$ (M= Zn, Fe, Ni). Mater. Sci. Poland **32**, 16–22 (2014)
Sedky, A., El-Brolossy, T.A., Mohamed, S.B.: Correlation between sintering temperature and properties of ZnO ceramic varistors. J. Phys. Chem. Solids **73**(3), 505–510 (2012)
Sedky, A., Amin, S.A., Mohamed, M.: Electrical, photoluminescence and ferromagnetic characterization of pure and doped ZnO nanostructures. Appl. Phys. A **125**, 308 (2019)
Sedky, A., Ali, A.M., Mohamed, M.: Structural and optical investigation of pure and Al doped ZnO annealed at different temperatures. Opt. Quantum Electron. **52**, 1–21 (2020)
Sedky, A., Ali, A.M., Somaily, H.H., Algarni, H.: Electrical, photoluminescence and optical investigation of ZnO nanoparticles sintered at different temperatures. Opt. Quantum Electron. **53**, 1–21 (2021)
Sedky, A., Afify, N., Ali, A.M., Algarni, H.: Structural, FTIR, optical and photoluminescence investigation of Zn1-xRExO nanoparticles for optical and power operation devices. J. Electroceram.. **49**(2), 33–52 (2022)
Sedky, A., Ali, A.M., Algarni, H.: Structural, FTIR, optical and dielectric properties of $Zn_{1-x}Al_xO$ ceramics for advanced applications. Opt. Quantum Electron. **54**(6), 376 (2022a)
Sedky, A., Ali, A.M., Algarni, H.: Structural, FTIR, optical and magnetic investigation of Zn1−xMxO ceramics with M= Cu, Mn: comparative study. J. Alloys Compd. **912**, 165139 (2022b)
Sedky, A., Mohamed, S.B.: Effect of temperature on the electrical properties of $Zn_{0.95}$ $M_{0.05}O$ (M = Zn, Fe, Ni). Mater. Sci. Poland **32**(1), 16 (2014)
Seetawan, U., Jugsujinda, S., Seetawan, T., Ratchasin, A., Euvananont, C., Junin, C., Thanachayanont, C., Chainaronk, P.: Effect of calcinations temperature on crystallography and nanoparticles in ZnO disk. Mater. Sci. Appl. **2**, 1302 (2011)
Shan, F.K., Liu, Z.F., Liu, G.X., Lee, W.J., Lee, G.H., Kim, I.S.: Aging and annealing efects of ZnO thin flms on GaAs substrates deposited by pulsed laser deposition. J. Electroceram. **13**, 195–200 (2004)
Srinet, G., Kumar, R., Sajal, V.: Properties of sol-gel derived Ni doped ZnO nanoparticles. J. Appl. Phys. **114**, 033912 (2013)
Srinivasan, N., Kannan, J.C.: Investigation on room temperature photoluminescence of pure and aluminum doped zinc oxide nanoparticles. Mater. Sci. Poland **33**, 205 (2015)
Srinivasulu, T., Saritha, K., Ramakrishna Reddy, K.T.: Synthesis and characterization of Fe-doped ZnO thin films deposited by chemical spray pyrolysis. Mod. Electron. Mater. **3**(2), 76–85 (2017)
Tariq, M., Li, Y., Li, W., Yu, Z., Li, J., Hu, Y., Zhu, M., Jin, H., Li, Y., Skotnicova, K.: Enhancement of ferromagnetic properties in (Fe, Ni) co-doped ZnO flowers by pulsed magnetic field processing. J. Mater. Sci. **30**, 8226–8232 (2019)
Tatsumi, T., Fujita, M., Kawamoto, N., Sasajima, M., Horikoshi, Y.: Intrinsic defects in ZnO films grown by molecular beam epitaxy. Jpn. J. Appl. Phys. **43**, 2602–2606 (2004)
Tripathy, S.K.: Refractive indices of semiconductors from energy gaps. Opt. Mater. Amst. **46**, 240 (2015)
Van Dijken, A., Meulenkamp, E.A., Vanmaekelbergh, D., Meijerink, A.: Identification of the transition responsible for the visible emission in ZnO using quantum size effects. J. Lumin. **90**(3–4), 123–128 (2000). https://doi.org/10.1016/S0022-2313(99)00599-2
Vanheusden, K., Warren, W.L., Seager, C.H., Tallant, D.R., Voigt, J.A., Gnade, B.E.: Mechanisms behind green photoluminescence in Zno phosphor powders. Jpn. J. Appl. Phys. **79**(10), 7983–7985 (1996)
Vvan Dijken, A., Meulenkamp, E.A., Vanmaekelbergh, D., Meijerink, A.: The kinetics of the radiative and nonradiative processes in nanocrystalline ZnO particles upon photoexcitation. J Phys Chem B. **104**(8), 1715–1723 (2000). https://doi.org/10.1021/jp993327z
Wang, Y.G., Lau, S.P., Lee, H.W., Yu, S.F., Tay, B.K., Zhang, X.H.: Hng, Photoluminescence study of ZnO films prepared by thermal oxidation of Zn metallic films in air. J. Appl. Phys. **94**, 354–358 (2003)
Wang, X.D., Zhou, J., Song, J.H., Liu, J., Xu, N., Wang, Z.L.: Piezoelectric field effect transistor and nanoforce sensor based on a single ZnO nanowire. Nano Lett. **6**, 2768–2772 (2006)
Wojnarowicz, J., Kusnieruk, S., Chudoba, T., Gierlotka, S., Lojkowski, W., Knoff, W., Lukasiewicz, M.I., Witkowski, B.S., Wolska, A., Klepka, M.T., et al.: Paramagnetism of cobalt-doped ZnO nanoparticles obtained by microwave solvothermal synthesis. Beilstein J. Nanotechnol. **6**, 1957–1969 (2015)
Wojnarowicz, J., Mukhovskyi, R., Pietrzykowska, E., Kusnieruk, S., Mizeracki, J., Lojkowski, W.: Microwave solvothermal synthesis and characterization of manganese-doped ZnO nanoparticles. Beilstein J. Nanotechnol. **7**, 721–732 (2016)

Wojnarowicz, J., Chudoba, T., Gierlotka, S., Sobczak, K., Lojkowski, W.: Size control of cobalt-doped ZnO nanoparticles obtained in microwave solvothermal synthesis. Curr. Comput.-Aided Drug Des. **8**, 179 (2018)
Xu, X.Y., Cao, C.B.: Structure and ferromagnetic properties of Co-doped ZnO powders. J. Magn. Magn. Mater. **321**, 2216–2219 (2009)
Xu, Q., Zhou, S., Schmidt, H.: Magnetic properties of ZnO nanopowders. J. Alloys Compd. **487**, 665–667 (2009)
Yang, Z.: A perspective of recent progress in ZnO diluted magnetic semiconductors. Appl. Phys. A **112**, 241–254 (2013)
Yong-Sheng, T., Ze-Bo, F., Wei, C., Pi-Mo, H.: Ferromagnetism in Eu-doped ZnO films deposited by radio-frequency magnetic sputtering. Chin. Phys. B. **19**(9), 097502 (2010). https://doi.org/10.1088/1674-1056/19/9/097502
Yu, J., Zhao, X., Zhao, Q.: Photocatalytic activity of nanometer TiO2 thin films prepared by the sol-gel methodMater. Chem. Phys. **69**, 25 (2001)
Zeyada, H.M., El-Ghamaz, N.A., Gaml, E.A.: Effect of substitution group variation on the optical functions of-5-sulfono-7-(4–x phenyl azo)-8-hydroxy quinoline thin films. Curr. Appl. Phys. **13**(9), 1960–1966 (2013)

Authors and Affiliations

A. Sedky[1] · N. Afify[1] · Abdullah Almohammedi[2] · E. M. M. Ibrahim[3] · Atif Mossad Ali[4]

N. Afify
afify@aun.edu.eg

[1] Department of Physics, Faculty of Science, Assiut University, Assiut 71516, Egypt

[2] Physics Department, Faculty of Science, Islamic University of Madinah, Aljamiah, Madinah 42351, Saudi Arabia

[3] Department of Physics, Faculty of Science, Sohag University, Sohag 82524, Egypt

[4] Department of Physics, Faculty of Science, King Khalid University, Abha, Saudi Arabia

Zhang, J., Li, X.Z., Shi, J., Lu, Y.F., Sellmyer, D.J.: Structure and magnetic properties of Mn-doped ZnO thin films. J. Phys. Condens. Matter **19**, 036210 (2007)
Zhang, J., Tse, K., Wong, M., Zhang, Y., Zhu, J.: A brief review of co-doping. Front. Phys. **11**, 117405 (2016)